Experimental investigation and gyrokinetic simulations of multi-scale electron heat transport in JET, AUG, TCV

A. Mariani,[1,2,*] N. Bonanomi,[3] P. Mantica,[2] C. Angioni,[3] T. Görler,[3] O. Sauter,[4] G.M. Staebler,[5] Eurofusion JET1 contributors,[†] Eurofusion MST1 contributors,[‡] ASDEX Upgrade team,[§] TCV team,[¶] and ITPA transport & confinement group[**]

[1]Department of Physics "G. Occhialini", University of Milano-Bicocca, Milano, Italy
[2]Institute for Plasma Science and Technology, CNR, Milano, Italy
[3]Max-Planck-Institut für Plasmaphysik, Garching, Germany
[4]École Polytechnique Fédérale de Lausanne (EPFL), Swiss Plasma Center (SPC), Lausanne, Switzerland
[5]General Atomics, San Diego, United States of America

(Dated: July 7, 2022)

Tokamaks dominated by electron heating like ITER could possibly suffer from the consequences of an electron temperature gradient (ETG) mode destabilisation, which could develop a turbulent electron heat flux capable of setting an upper limit to the achievable electron temperature peaking, resulting in a degradation of the fusion performances. An effort is carried out in the paper to collect and compare the results of dedicated plasma discharges performed during the last years at three of the major European tokamaks, TCV, AUG and JET, by analysing the electron heat transport for cases presumably compatible with ETGs relevance given the actual theoretical understanding of these instabilities. The response of the electron temperature profiles to electron heat flux changes is experimentally investigated by performing both steady state heat flux scans and perturbative analysis by radio frequency modulation. The experimental results are confronted with numerical simulations, ranging from simpler linear gyrokinetic or quasi-linear runs, to very computationally expensive nonlinear multi-scale gyrokinetic simulations, resolving ion and electron scales at the same time. The results collected so far tend to confirm the previously emerging picture indicating that only cases with a proper balance of electron and ion heating, with similar electron and ion temperatures and sufficiently large electron temperature gradient, are compatible with a non negligible impact of ETGs on the electron heat transport. The ion heating destabilises ETGs not only by increasing the ion temperature but also thanks to the stabilisation of ion-scale turbulence by a synergy of fast ions and $E \times B$ shearing which are in some cases associated to it. The stabilising effect of plasma impurities on ETGs is still under investigation by means of multi-scale gyrokinetic simulations, and also direct experimental measurements of density and temperature fluctuations at electron scales would be needed to ultimately assess the impact of ETGs.

I. INTRODUCTION

Improving the knowledge of the electron heat transport properties in tokamaks is gaining importance in view of designing new devices like ITER, which will be dominated by electron heating due to electron cyclotron resonance heating (ECH) and alpha heating. Indeed, with the fusion power being proportional to the square of the ion temperature at a given density, the only way to obtain optimal performance in such devices is connected with the capacity of indirectly heating ions by collisional heat exchange from electrons. Therefore, a hypothetical incapacity to heat electrons would result in poor fusion performance. This is directly connected to the concept of 'temperature stiffness', which refers to the degree to which the radial temperature profiles respond to changes in the applied heat fluxes. A 'stiff' electron temperature profile, i.e. a T_e profile which does not peak when increasing the applied electron heat flux $q_{e,ext.}$, due to the development of a turbulent outward radial heat flux which balances $q_{e,ext.}$, could be detrimental to these devices. The study of the generation of a possible strong turbulent electron transport leading to a high electron stiffness, depending on plasma parameters, is thus a key point. In general, the observed levels of turbulent transport in tokamak plasmas, in both the ion and electron channels, are the result of drift-wave micro-instabilities driven by the free energy available in the plasma pressure gradients. In particular, core transport in present tokamaks is currently mostly ascribed to turbulence driven by the nonlinear (NL) saturation of ion-scale micro-instabilities ($k_\theta \rho_i \leq 1$, where k_θ is the poloidal wave number and ρ_i the ion Larmor radius), such as the ion temperature gradient (ITG) modes, which are driven by the logarithmic gradient of the ion temperature $\nabla \ln T_i$, and the trapped electron modes (TEM), driven by both the logarithmic gradients of the electron temperature $\nabla \ln T_e$ and the electron density $\nabla \ln n_e$. In particular, the turbulence generated by the NL saturation of TEM is a source of 'electron temperature stiffness' for sufficiently large values of the TEM drive, resulting in an upper boundary for the normalised T_e logarithmic gradient $R/L_{Te} = -R\nabla T_e \cdot \hat{r}/T_e$ ($\hat{r}$ radial unit vector), with R the plasma major radius. However, it has been shown that electron temperature gradient (ETG) modes

* Electronic address: alberto.mariani@istp.cnr.it
† See the author list of 'Overview of JET results for optimising ITER operation' by J. Mailloux et al to be published in Nuclear Fusion Special issue: Overview and Summary Papers from the 28th Fusion Energy Conference (Nice, France, 10-15 May 2021) for the Eurofusion JET1 conributors.
‡ See Labit et al. 2019 (https://doi.org/10.1088/1741-4326/ab2211) for the Eurofusion MST1 contributors.
§ See Meyer et al. 2019 (https://doi.org/10.1088/1741-4326/ab18b8) for the TCV team.
¶ See Coda et al. 2019 (https://doi.org/10.1088/1741-4326/ab25cb) for the Eurofusion JET1 conributors.
** See https://portal.iter.org/departments/POP/ITPA/TC/Pages/default.aspx for the ITPA transport & confinement group.

[1], which can be destabilized at electron-scales by increasing R/L_{Te}, can also impact the electron heat transport, both by directly producing a turbulent q_e and by exchanging energy with lower-k_θ ITG-TEM turbulence through multi-scale coupling [2–8]. Therefore, the relative role of TEM and ETG in setting an upper boundary for the electron temperature peaking has to be determined depending on plasma parameters. ETGs could play a role in the electron heat transport when mixed ion and electron heating is applied to plasmas. For these cases, a proper balance of ion heating, decreasing the ETG R/L_{Te} linear threshold (proportional to $(1 + Z_{\text{eff}}T_e/T_i)$[9], where Z_{eff} is the effective charge), and electron heating (pushing R/L_{Te} towards threshold while increasing the threshold due to T_e/T_i increase), could destabilize them, possibly leading to similar R/L_{Te} thresholds for TEM and ETGs. Also all mechanisms that stabilize ITGs, such as $E \times B$ shearing or fast ions (FI) from neutral beam injection (NBI) and/or ion cyclotron resonance heating (ICH), may open a favourable window for ETG destabilization due to multi-scale interactions. Moreover FI can linearly destabilize ETGs due to FI contribution to T_i/T_e. A great effort is actually devoted to analyse different machines, comparing experimental and numerical results, within the framework of EUROfusion and of the ITPA Transport & Confinement group. In this paper, the analysis of plasmas of three different tokamaks, i.e. the Joint European Torus (JET, at Culham, UK), ASDEX Upgrade (AUG, at Garching, DE) and the Tokamak à Configuration Variable (TCV, at Lausanne, CH), is presented. Dedicated plasma discharges have been analysed experimentally and modelled numerically, by means of gyrokinetic (GK) codes (GENE [10, 11] and GKW [12]) and the reduced quasi-linear model TGLF [13].

Two dedicated L-mode discharges, with $B_0 = 1.41T$, $I_p = 170kA$ have been performed in TCV with a different proportion of deposited ECH ($\sim 0.4 - 0.7MW$) power on- vs off-axis to perform a heat flux scan. Each pulse presented different phases corresponding to a different proportion of NBI($\sim 1MW$)/ECH power to vary T_e/T_i, with ECH both steady and modulated to allow a perturbative analysis. The TCV results that we include in this paper are published in [4]. Here the focus is on the comparison with AUG and JET. Similar experiments have been carried out in AUG [5, 14], producing H-mode discharges with $B_0 = 2.6T$, $I_p = 0.8MA$, injecting $2.5MW$ of ECH (steady and modulated) and $5MW$ of NBI in order to have $T_e \sim T_i$, varying the ECH radial deposition (heat flux scan). Following early results pointing to an important role of ETGs in JET [3], very recently dedicated sessions on ETGs have also been performed at JET. Both L- and H-mode plasmas have been obtained, with $B_0 = 3.3T$, $I_p = 2MA$, injecting $0 - 20MW$ of NBI and up to $6MW$ of ICH (H minority with $n_H/n_e \sim 6\%$, to mainly heat electrons), achieving heat flux scans for a range of T_e/T_i values. The main JET results that we included in our comparison are submitted to publication [15]. A detailed review and comparison of these cases, concerning the experimental and numerical analysis of the impact of ETGs on electron heat transport, including the new multi-scale GK analysis of the selected AUG reference discharge, is the focus of this paper. The radial position $\rho_{tor} = 0.5$ has been considered for all the pulses and devices.

II. EXPERIMENTAL RESULTS

The response of the T_e profiles to the applied heating can be experimentally investigated by performing normalized electron heat flux scans and/or radio frequency (RF) power modulation analysis. The two methods can be used in conjunction to extract information on the dependence of the gyro-Bohm (gB) normalized electron heat flux $q_{e,gB}$ on R/L_{Te}, yielding experimental values for the threshold $R/L_{Te,crit.}$ for the onset of turbulent transport and for the 'electron stiffness' $\partial q_{e,gB}/\partial R/L_{Te}$. Here the heat flux in gB units is defined as $q_{j,gB} = q_j(e^2R^2B_0^2/\sqrt{m_i}n_eT_e^{5/2})$, where $j = e, i$ indicate electrons or ions, q_j is the radial heat flux per unit surface, e the electron charge, m_i the ion mass and B_0 the vacuum magnetic field on the magnetic axis. Steady state scans have been obtained for TCV, AUG and JET, corresponding to the experiments that have been summarized in the introduction. RF (ECH) modulation measurements have been obtained for TCV and AUG (for JET the use of ICH H minority heating prevented the use of ICH modulation due to too broad deposition profiles and too long FI slowing down times). The results at $\rho_{tor} = 0.5$ are shown in Fig.1 (a)-(c) for the three machines.

For TCV, the comparison of points with on- vs off-axis ECH indicates moderate stiffness for both ECH only (red) and mixed NBI-ECH case (black). Only the perturbative analysis allows to measure an ETG-compatible local stiffness for the mixed NBI-ECH point ($T_e \sim T_i$) with ECH on-axis (magenta line), which becomes the best candidate to show an ETG contribution to q_e. All the experimental points of the AUG heat flux scan with $T_e \sim T_i$ are shown in Fig.1 (b). Similarly to TCV, the steady state scan trend is compatible with TEM stiffness. However, the local slope has been evaluated using RF modulation for pulse #31506 (largest $q_{e,gB}$) and it is compatible with ETG presence. Unfortunately, for both TCV and AUG there is a lack of higher $q_{e,gB}$ points which could show the actual presence of an 'ETG wall'. For JET (Fig.1 (c)), the $T_e/T_i = 0.9$ high-pedestal H-modes (red) are stuck to low $q_{e,gB}$ due to gB normalisation (high T_e), while the $T_e/T_i = 1.3$ L-modes (blue) present a mild TEM-consistent stiffness. Thus only the $T_e \sim T_i$ low-pedestal H-modes and L-modes (black) are compatible with a possible ETG wall due to the highest $q_{e,gB}$ pulse #95457. Despite the JET scan with $T_e \sim T_i$ is compatible with an 'ETG wall' picture, it lacks RF modulation data to compare with. Comparing the three tokamaks, hence confirms that the best candidates to show a possible ETG role in producing q_e are the ones with a balance of ion and electron heating, leading to a concomitance of $T_e \sim T_i$ and large R/L_{Te}.

III. LINEAR MULTI-SCALE GYROKINETIC RESULTS

Linear multi-scale simulations at mid-radius ($\rho_{tor} = 0.5$) have been performed in order to characterise the turbulence regime using the GENE code for the TCV, AUG and JET

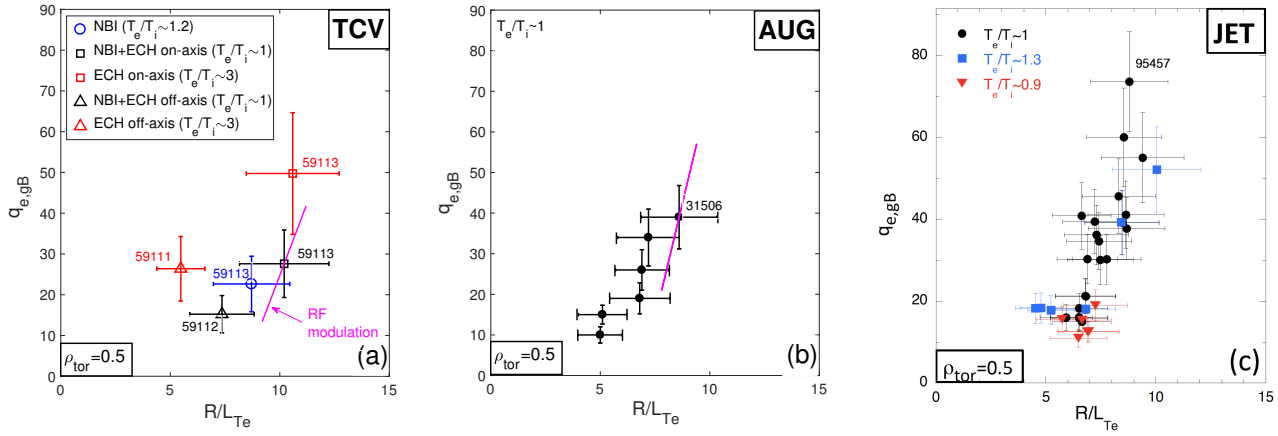

Figure 1. Experimental electron heat flux scans at mid-radius $\rho_{tor} = 0.5$ for TCV (a), AUG (b) and JET (c). The electron heat flux in gB units $q_{e,gB}$ is shown versus R/L_{Te}. After [4] (a), [5, 14] (b), [15] (c).

	TCV ECH (59113)	TCV ECH+NBI (59113)	TCV NBI (59113)	AUG (31506)	JET (95457)
T_e/T_i	3.04	~1	1.16	~1	~1
Z_{eff}	2.50	2.80	2.80	1.4	1.5
R/L_{Te}	10.59	10.20	8.71	8	9
R/L_{Ti}	5.94	5.55	15.07	6.5	4.59
R/L_{ne}	3.69	4.85	6.07	0.91	3.12
q	1.65	1.34	1.42	2.07	1.82
$\hat{s}$	0.99	1.19	1.14	6.85	1.05
β_e [10^{-3}]	2.01	2.37	1.54	5	1.12
ν_c [10^{-3}]	0.91	1.33	1.77	1.87	0.57
γ_E [c_s/R]	~0	0.14	0.34	0.04	~0

Table I. Main plasma parameters for the analised pulses at $\rho_{tor} = 0.5$.

cases. Some AUG simulations are similar to the ones that have been previously shown in [5], obtained using GKW with results that are consistent with the GENE ones.

GENE solves the GK equations coupled with the Maxwell equations within a δf approximation, using a set of field-aligned coordinates $\{x, y, z, v_{\|}, \mu\}$ in the reduced 5-dimensional GK phase space. x, y and z are the radial, binormal and parallel (to B) coordinates in configuration space, while $v_{\|}$ and μ are the parallel velocity and the magnetic moment. The simulations are carried out in the flux-tube limit using realistic geometries, reconstructed using numerical equilibria from CHEASE [16] (TCV) and EFIT [17] (AUG, JET), taking into account collisions and finite-β (electromagnetic) effects. The pulses with largest $q_{e,gB}$ (best candidates to show an ETG impact to q_e), are selected for AUG (#31506, H-mode) and JET (#95457, L-mode), while all the cases with ECH on-axis and the NBI only case (for comparison) for TCV (3 phases from #59113, L-mode). The main plasma parameters of the selected cases are listed in Table I.

Here, in particular, the GENE collisional parameter ν_c is listed instead of the electron-ion thermal collision rate $\nu_{ei} = 4(n_i/n_e)\sqrt{T_e/m_e}\nu_c/R$, since ν_c depens only on the measured quantities n_e and T_e while ν_{ei} changes given the number of considered species (n_i adapted invoking neutrality). The impurities which cause Z_{eff} in the three tokamaks are C (TCV), B and W (AUG) and Be, C, Ne, Ni and W (JET). For consistency with the JET NL multi-scale GK simulation, where it was impossible to include three kinetic impurities for lack of computational resources, impurities are taken into account in the simulations using a single C species, to reproduce the experimental Z_{eff} and ion dilution as well as possible without increasing the cost of the simulations. This has been done in both AUG and JET simulations when impurities are taken into account. Finally, $\gamma_E = -(x/q)(\partial\Omega_{tor}/\partial x)R/c_s$ is the $E\times B$ shearing rate, where Ω_{tor} is the toroidal angular velocity and $c_s = \sqrt{T_e/m_i}$ the ion sound speed.

All the cases are found to be ITG-dominant at ion-scales except those from TCV when ECH is injected, which are TEM-dominant. ETGs are found unstable at electron scales. The impact of ETGs on q_e can be roughly predicted using a simple criterion, which states that ETGs should contribute to q_e if the peak of the ratio γ/k_y of the growth rate of the most unstable mode and the corresponding poloidal wavenumber is larger at electron-scales than at ion-scales [18]. γ/k_y is shown versus k_y for TCV, AUG and JET cases in Fig.2 (a), (b) and (c) respectively.

For AUG, the lower $R/L_{Ti} = 3.65$ value has been considered together with the experimental one ($R/L_{Ti} = 6.5$), since it is the value which has been considered in the NL GK multi-scale simulations (see Sec.V), being the R/L_{Ti} which allows to match the experimental q_i with ion-scale NL simulations (see Sec. IV). For JET, instead of the experimental $R/L_{Ti} = 4.59$, the two values $R/L_{Ti} = 5.17, 5.77$ are considered, which allow to match the experimental q_i at the two ends of its error bar with ion-scale NL GK simulations (see Sec.IV), to test the sensitivity to R/L_{Ti} (NL GK multi-scale simulations have been run with both the R/L_{Ti} values for JET, see Sec.V). For TCV the ETG-relevance criterion is only met for the mixed

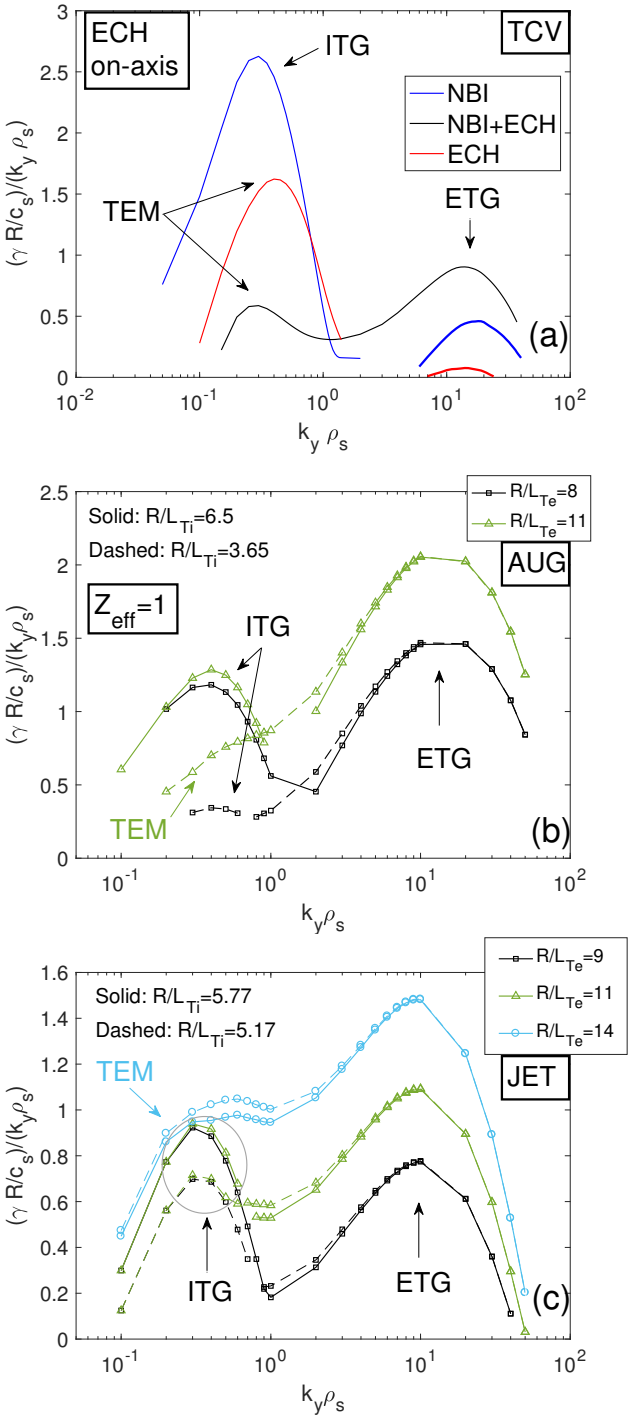

Figure 2. Linear GENE scans of γ/k_y, normalised with $\rho_s c_s/R$ ($\rho_s = c_s/\Omega_i$ is the ion Larmor radius, where ω_i is the ion cyclotron frequency) for the selected TCV (a), AUG (b) and JET (c) cases. The TCV parameters are taken from pulse 59113, while for JET they are consistent with pulse 95467. After [4] (a), [15] (c)

NBI-ECH case, as expected. In particular, the condition is fulfilled because of a strong linear stabilisation of ion-scale TEMs by NBI FI ($n_{FI}/n_e \sim 10\%$, $T_{FI}/T_e \sim 16$, $R/L_{n,FI} \sim 14$, $R/L_{T,FI} \sim 2$). For AUG, the criterion is always met. In particular, the ion-scales are strongly suppressed at the lower value of R/L_{Ti}, indicating a possible strong role of ETGs for that case. Similar simulations have been run with GKW for AUG, and the results are published in [5] (see Fig.19), indicating a role for ETGs for $R/L_{Te} \geq 6$ at experimental R/L_{Ti}. The AUG runs just give a lower boundary for the ETG R/L_{Te} threshold, since they set $Z_{\rm eff} = 1 < 1.4 = Z_{\rm eff,exp.}$, thus already underpredicting the linear threshold by $\sim 20\%$. $Z_{\rm eff} = 1$ is kept for AUG consistently in linear, NL ion-scale and NL multi-scale runs, since it was impossible to use the exp. value of $Z_{\rm eff}$ in the NL multi-scale runs due to insufficient computational resources. However, the impact of impurities has also been evaluated for AUG, by means of linear GK simulations (see the following paragraph) and using a faster quasi-linear model (see Sec. VI). For JET, FI (from NBI and ICH) have been neglected since $n_{FI}/n_e \sim 0.2\%$ at $\rho_{tor} = 0.5$. JET results predict a non-negligible contribution of ETGs to q_e for $R/L_{Te} \geq 11$ when $R/L_{Ti} = 5.77$ and for $R/L_{Te} \geq 9$ when $R/L_{Ti} = 5.17$.

In order to test the dependence of the AUG and JET results on $Z_{\rm eff}$, linear scans of γ/k_y vs k_y have been performed at fixed k_y values, comparing the results obtained setting experimental $Z_{\rm eff}$ with the ones coming from simulations where impurities are neglected ($Z_{\rm eff} = 1$). The same two couples of R/L_{Ti} values $R/L_{Ti} = 3.65, 6.5$ and $R/L_{Ti} = 5.17, 5.77$ are considered for AUG and JET respectively, as in Fig.2 (b) and (c). The results are shown in Fig.3 where, following [5] (see Fig.20), for each case the γ/k_y corresponding to two sets of k_y are compared, the first around the γ/k_y maximum at ion scales (black/blue), the second around the γ/k_y maximum at electron scales (red/magenta). The ETG relevance criterion is met for $R/L_{Te} > R/L_{Te,crit.}$, where $R/L_{Te,crit.}$ can be directly visualised looking at the figure, as the R/L_{Te} so that the upper end of the electron-scale 'stripe' crosses the upper end of the ion-scale 'stripe'. The plots on the left indicate AUG results, while the plots on the right indicate JET ones. Moreover, the upper plots correspond to the larger considered R/L_{Ti} for each case, while the lower plots correspond to the smaller R/L_{Ti}. Finally, the results obtained with $Z_{\rm eff} = 1$ are indicated by squares, while the ones with $Z_{\rm eff,exp.}$ are shown by triangles. It can be seen that, as expected from linear physics (ETG linear threshold proportional to $1+Z_{\rm eff}T_e/T_i$), $R/L_{Te,crit.}$ is larger for larger $Z_{\rm eff}$. The impact of $Z_{\rm eff}$ is small-moderate $\Delta(R/L_{Te,crit.}) = R/L_{Te,crit.}(Z_{\rm eff} = Z_{\rm eff,exp.}) - R/L_{Te,crit.}(Z_{\rm eff} = 1) \sim 1$ for the larger R/L_{Ti} cases ((a) and (b)), while it is small $\Delta(R/L_{Te,crit.}) < 0.5$ for the smaller R/L_{Ti} cases ((c) and (d)). It has also to be noted that collisions, at similar $Z_{\rm eff}$, are more effective in stabilising ion scales for the JET case.

More details on part of the simulations that are shown in this section can be found in [4], [5], [15], corresponding to TCV, AUG and JET cases, respectively. This also holds for the TCV results of Sec. VI and the JET results of Sections IV and VI. Regarding AUG, part of the the GENE linear and all the NL multi-scale GK results are published here for the first time.

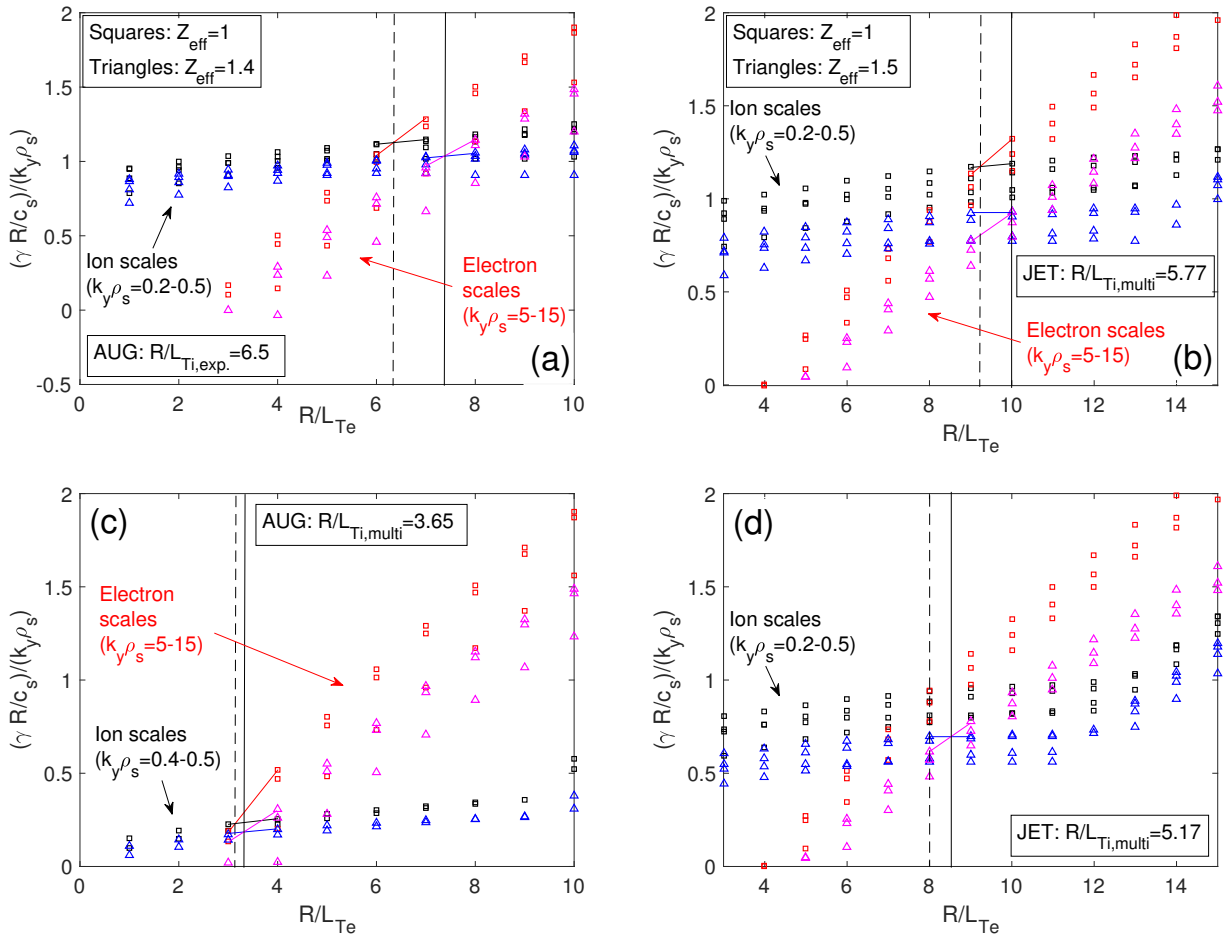

Figure 3. Effect of $Z_{\rm eff}$ on ETG impact: GENE linear γ/k_y ratio vs R/L_{Te} for JET (left) and AUG (right) cases, for selected k_y intervals corresponding to ion scale (black/blue) and electron scale (red/magenta) γ/k_y peaks. Two values of R/L_{Ti} are considered for each case (different rows), as well as two values of $Z_{\rm eff}$ ($Z_{\rm eff}$ = 1: squares, reference $Z_{\rm eff}$: triangles). The dashed and solid vertical lines indicate the R/L_{Te} corresponding to the crossing of electron-scale and ion-scale γ/k_y stripes, for $Z_{\rm eff}$ = 1 and reference $Z_{\rm eff}$ respectively.

IV. NON-LINEAR ION-SCALE GYROKINETIC RESULTS

GENE NL ion-scale simulations have been performed to interpret the experimental results, in order: 1) to test if the GK flux levels match the experimental ones, or a contribution from ETGs (lacking in ion-scale runs) is needed; 2) to compare the GK stiffness with the experimental one, evidencing a possible ETG role if the experimental stiffness is underpredicted by ion-scale GK. Both electron and ion heat channels are investigated for AUG and JET, where the ion-scale is ITG-dominant and very sensitive to R/L_{Ti}, while only the electron channel is investigated for TCV where TEMs are dominant at ion-scales. The TCV GK results are shown by black and red diamonds in Fig.4 (a), corresponding to ECH only and mixed ECH-NBI cases, respectively.

Two GK simulations have been performed for each experimental case: the first with experimental parameters and the second reducing R/L_{Te} from $\sim$ 10 to 7, to evaluate the stiffness. The experimental points with ECH off-axis (lower R/L_{Te}) have been kept in the figure to give an idea of the experimental stiffness. However, the GK runs have been done with parameters from the cases with ECH on-axis (pulse #59113), therefore GK and experimental stiffness should be only qualitatively compared. It follows that GK explains both the flux levels and the stiffness for the ECH only case, while for the mixed ECH-NBI case GK both strongly under-predicts the flux levels and the stiffness, invoking the ETGs as a possible player to fill those gaps. In particular, a synergy of FI and $E\times B$ stabilisation ($\gamma_E \sim 0.14$) is observed for this case, reducing the TEM-driven $q_{e,gB}$ to negligible values compared to the experimental ones. Two NL runs have been performed for the AUG case, varying $R/L_{Te} = 8, 11$. They are indicated by blue diamonds in Fig.4 (b). The experimental points of the R/L_{Te} scan with $T_e \sim T_i$ have all been kept in the figure (black dots with error bars) in order to give an idea of the experimental local stiffness, while the GK simulations have been run with the parameters from pulse #31506. The logarithmic gradient of T_i has been set to $R/L_{Ti} = 3.65 < 6.5 = R/L_{Ti,exp.}$ in order to match the experimental value of $q_{i,gB}$ with GK (see the smaller picture in Fig. 3 (b)). This is needed since the T_i profile is very stiff with respect to q_i variations, due to ITG-

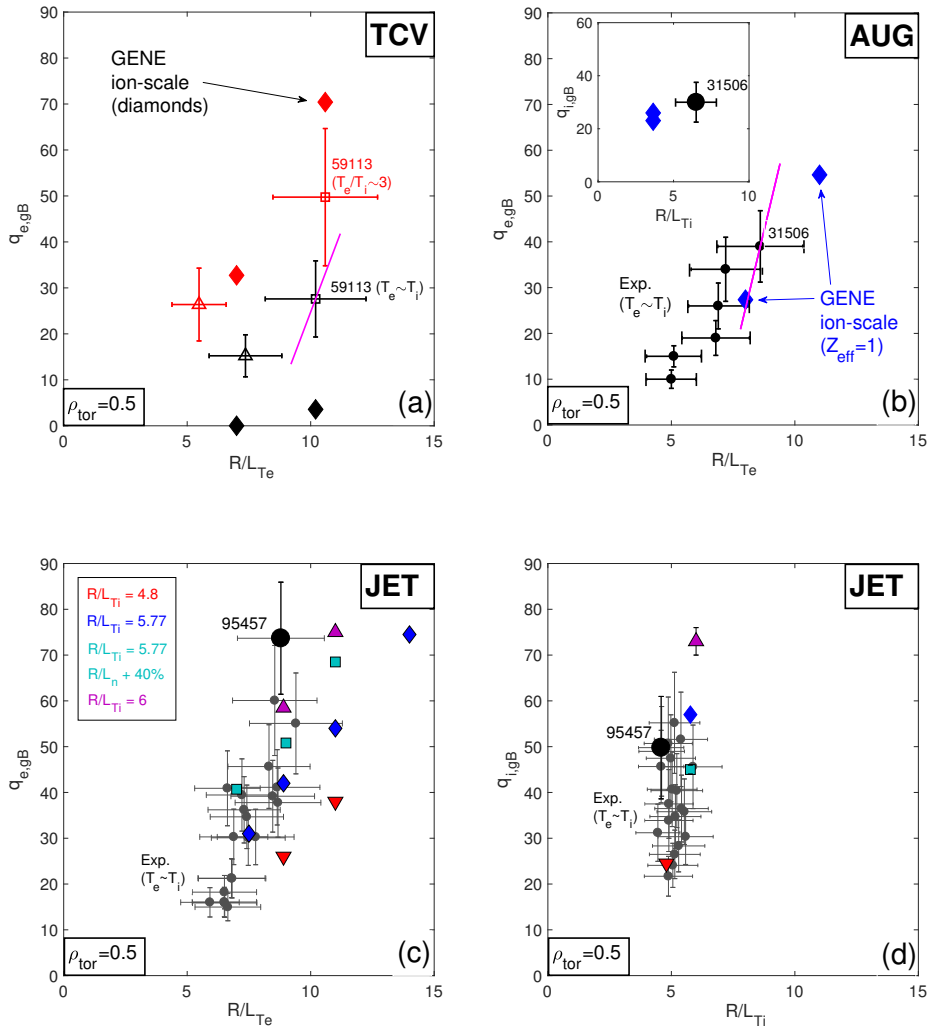

Figure 4. GENE NL ion-scale $q_{e,gB}$ vs R/L_{Te}, compared with the exp. results of Fig.1, for TCV (a), AUG (b) and JET (c). GENE NL ion-scale $q_{i,gB}$ vs R/L_{Ti} is indicated for AUG in the small box in (b), while it is shown in (d) for JET. The TCV case with NBI only is not shown as well as the JET exp. cases with $T_e \neq T_i$. After [4] (a), [5, 14] (b), [15](c)/(d).

dominant ion scales. Moreover, impurities and $E \times B$ shear ($\gamma_E \sim 0.04$) have been neglected, to better compare with the multi-scale run (see Sec. V). For the same reason, FI have not been included ($n_{FI}/n_e \sim 1\%$, $T_{FI}/T_e \sim 15$, $R/L_{n,FI} \sim 6$, $R/L_{T,FI} \sim 2$). However, since for this case the FI density fraction is 10 times smaller than the TCV ECH+NBI case and the γ_E is 3.5 times smaller, one should expect a significantly smaller impact of FI and $E \times B$ shear on NL fluxes than for TCV. The results of the simulations show that even if for the AUG case the experimental $q_{e,gB} = 39$ is only moderately under-predicted by GK ($q_{e,gB} = 27.4$, slightly below the ±20% error bar), the experimental stiffness (from RF modulation: magenta line) is strongly under-predicted. Turning to JET results (Fig.4 (c) and (d), corresponding to the electron and ion channels, respectively), Three R/L_{Ti} were considered in the GK runs ($R/L_{Ti} = 4.8, 5.77, 6$: red, blue and magenta, respectively) and scans in R/L_{Te} were performed for each value of R/L_{Ti}. Only the experimental points of the R/L_{Te} scan with $T_e \sim T_i$ have all been kept in the figure in order to give an idea of the experimental local stiffness, while the GK simulations have been run with the parameters from pulse #95467. As visible in Fig.4 (d), the ion heat flux is very stiff in R/L_{Ti}, due to ITGs. Changing R/L_{Ti} also impacts q_e, which increases by $\sim 100\%$ when changing R/L_{Ti} from 4.88 to 6. However, changing R/L_{Ti} does not impact the R/L_{Te} stiffness of q_e. For $R/L_{Ti} = 5.77$, a study of the effect of R/L_{ne} was also performed, increasing the nominal value by 40%. When increasing R/L_{ne}, $q_{e,gB}$ increases by about 40% due to stronger TEMs, while q_i decreases, without changing the R/L_{Te} stiffness of q_e. Summarizing these JET results, while the single experimental point can be reproduced by varying the input parameters within error bars in GK simulations, the experimental slope of $q_{e,gB}$ vs R/L_{Te} is underestimated by ion-scale GK. A mechanism providing a q_e contribution scaling with R/L_{Te} would

be needed, which could come from ETGs.

V. NON-LINEAR MULTI-SCALE GYROKINETIC RESULTS

Collecting the results from the three tokamaks, it seems that for the cases with $T_e \sim T_i$ the ion-scales are not sufficient to explain the experimental flux levels and/or the T_e stiffness. As a consequence, dedicated multi-scale NL GENE runs have been performed to quantify the contribution of ETGs to both q_e and to its slope vs R/L_{Te}, for AUG and JET. This has not yet been done for TCV, since the priority has been given to larger tokamaks where $\rho^* = \rho_i/a$ effects (called 'global' effects, where ρ_i is the ion Larmor radius and a the plasma minor radius), which are not retained in the GENE flux-tube version, should not play a role. Actually, a global multi-scale NL GK simulation would require more than our available computational resources. For AUG, the same parameters of the ion-scale runs (thus with $Z_{\rm eff} = 1$), have been kept. To reduce the computational cost of these heavy runs, the initial NL saturation phase for the $R/L_{Te} = 8$ run has been performed including only the ion scales, keeping the same parameters and the same number of k_x modes needed for the corresponding multi-scale. Then, after the NL convergence of the fluxes, the k_y grid has been expanded ($n_{ky} = 32 \rightarrow 512$) to include electron scales. The multi-scale run at larger $R/L_{Te} = 11$ has been initialised changing R/L_{Te} starting from a checkpoint of the $R/L_{Te} = 8$ simulation. The radial and binormal box sizes for AUG are $[L_x, L_y] = [118.2, 83.8]\rho_s$, corresponding to $k_{y,min}\rho_s = (2\pi/L_y)\rho_s = 0.075$, $k_{x,min}\rho_s = (2\pi/L_x)\rho_s = 0.053$. The simulations have been run with $[n_{kx}, n_{ky}, n_z, n_{v\|}, n_\mu] = [1280, 512, 32, 32, 12]$ grid points. The results of the AUG multi-scale simulations (red stars) are compared with the ion-scale fluxes (blue diamonds) in Fig.5 (a).

The corresponding q_e spectra are presented in Fig.6 (a).

The impact of ETGs, coming from electron scales ($k_y\rho_s > 1$), on q_e, increases with increasing R/L_{Te}. It is moderate/large ($\sim 33\%$) at experimental $R/L_{Te} = 8$, while it becomes large ($\sim 55\%$) at $R/L_{Te} = 11$. The multi-scale stiffness in particular is well aligned with the RF modulation result (magenta). The observed moderate/large impact of ETGs for AUG case is thus in line with the linear prediction of ETGs impacting q_e for $R/L_{Te} > 6$, being both the considered R/L_{Te} values beyond 6.

Following the same strategy, three multi-scale runs have been performed for the JET case for $R/L_{Te} = 9, 11, 14$, with $R/L_{Ti} = 5.77$. For the JET case, impurities have been accounted for, the same way as in ion-scale NL and linear runs. The x and y box sizes have been set to $[L_x, L_y] = [88.6, 83.8]\rho_s$, corresponding to $k_{y,min}\rho_s = (2\pi/L_y)\rho_s = 0.075 \sim k_{x,min}\rho_s = (2\pi/L_x)\rho_s = 0.071$, and $[n_{kx}, n_{ky}, n_z, n_{v\|}, n_\mu] = [1536, 512, 32, 32, 12]$ grid points have been used. The results, shown in Fig.5 (b)/(c) and Fig.6 (b), indicate a negligible ($\sim 5\%$) impact of ETGs on q_e at experimental $R/L_{Te} = 9$, increasing with R/L_{Te} but remaining moderate ($\sim 18\%$) at $R/L_{Te} = 14$, in line with the linear prediction of an ETG impact for $R/L_{Te} > 11$ when $R/L_{Ti} = 5.77$. The stiffness of the multi-scale fluxes still does not explain the experimental slope.

Following the analysis of Figs.2 and 3, that indicates a larger role for ETGs at smaller R/L_{Ti} based on the γ/k_y criterion introduced in Section III, an additional multi-scale simulation has been run for the intermediate $R/L_{Te} = 11$ setting the lower $R/L_{Ti} = 5.17$ value that allows to match q_i at the lower boundary of its experimental error bar with ion-scale NL runs. This is done to check if indeed a larger impact of ETGs on q_e is observed in the multi-scale simulation by decreasing R/L_{Ti}, and if it could help to get closer to the experimental electron heat flux level. The results are shown in red in Fig.7, for the electron and ion channels in Fig.7 (a) and (b), respectively. The corresponding q_e spectra are shown in Fig.7 (c).

The results indicate that despite the ETG fraction is increasing with decreasing R/L_{Ti}, the decrease of the q_e fraction coming from ion-scales is larger, so that the overall q_e is smaller for $R/L_{Ti} = 5.17$ than for $R/L_{Ti} = 5.77$. The comparison of the q_e spectra corresponding to $R/L_{Ti} = 5.77$ (blue) and $R/L_{Ti} = 5.17$ (red) in Fig.7 (c), in particular, indicates that ETGs contribution to q_e increases only by 10% with decreasing R/L_{Ti}, going from 10% for $R/L_{Ti} = 5.77$ to 20% for $R/L_{Ti} = 5.17$. Summarising these multi-scale GK results, it is not possible to match both experimental values of q_e and q_i by first matching q_i within its experimental error bar with ion-scale simulations and then performing multi-scale runs to re-compute q_e and q_i. It could still be possible that some cross-scale effect like the one observed in [2], consisting in a backward effect of ETGs on ion scales when ion scales are marginally stable, could allow to match both the electron and ion heat fluxes with multi-scale simulations further lowering R/L_{Ti} closer to the ITG threshold. However, the very high ion stiffness of the experimental points seems to indicate that this last picture should not be likely for the considered JET case, since the cross-scale effect observed in [2] should imply a reduction of the ion stiffness. Moreover, for this 'high ion stiffness' case, the search of an 'optimal' value of R/L_{Ti} close to the ITG threshold to observe such cross-scale effect would require a fine R/L_{Ti} scan of such very heavy GK NL multi-scale simulations, which is beyond both the scope of this work and the available computational resources.

VI. MULTI-SCALE TGLF STAND-ALONE RESULTS

R/L_{Te} scans have been performed with the stand-alone version of TGLF for AUG and JET starting from reference parameters (Table I). The two most recent versions of TGLF have been used: TGLF SAT1-geo (11/2019: improved description of geometrical effects and calibration against GK with respect to SAT1 [13]) and SAT2 [19]. These scans have been run with the aim of further evaluating the impact of the impurities on the results. Comparing the two TGLF runs for AUG (blue and green in Fig.8 (a) for $Z_{\rm eff} = 1$ and $= 1.4$ respectively), the effect of impurities on the ETG wall is not negligible, but however TGLF with both $Z_{\rm eff} = 1$ and $= 1.4$ agrees with the experimental flux within the R/L_{Te} error bar and agrees with both the experimental stiffness (RF modulation: magenta) and the GENE multi-scale stiffness (red stars).

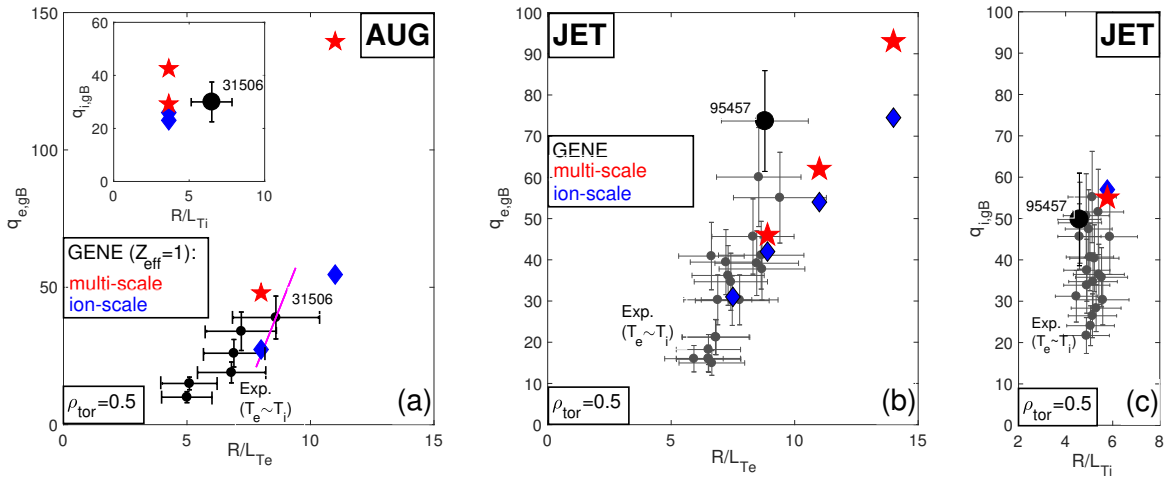

Figure 5. Multi-scale GENE electron heat flux in gB units $q_{e,gB}$ vs R/L_{Te} (red stars), compared with the corresponding ion-scale fluxes (blue diamonds), for AUG (a) and JET (b). Corresponding ion heat flux in gB units $q_{i,gB}$ vs R/L_{Ti} in (a) (small box) and (c). After [15] (b)-(c).

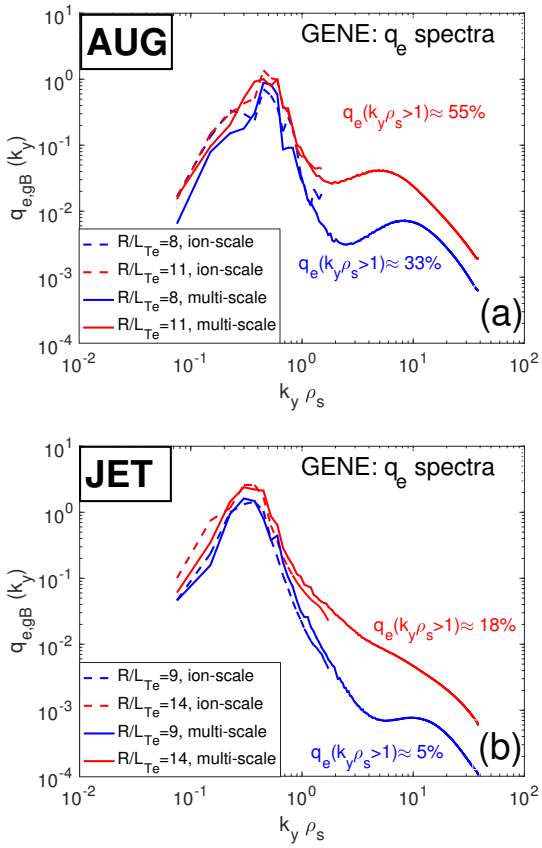

Figure 6. Electron heat flux spectra in gB units $q_{e,gB}(k_y)$, satisfying $q_{e,gB} = \sum_{k_y} q_{e,gB}(k_y)$, corresponding to the multiscale simulations of AUG (a) and JET (b) with extreme values of R/L_{Te}, i.e. $R/L_{Te} = 8, 11$ for AUG and $R/L_{Te} = 9, 14$ for JET. After [15].

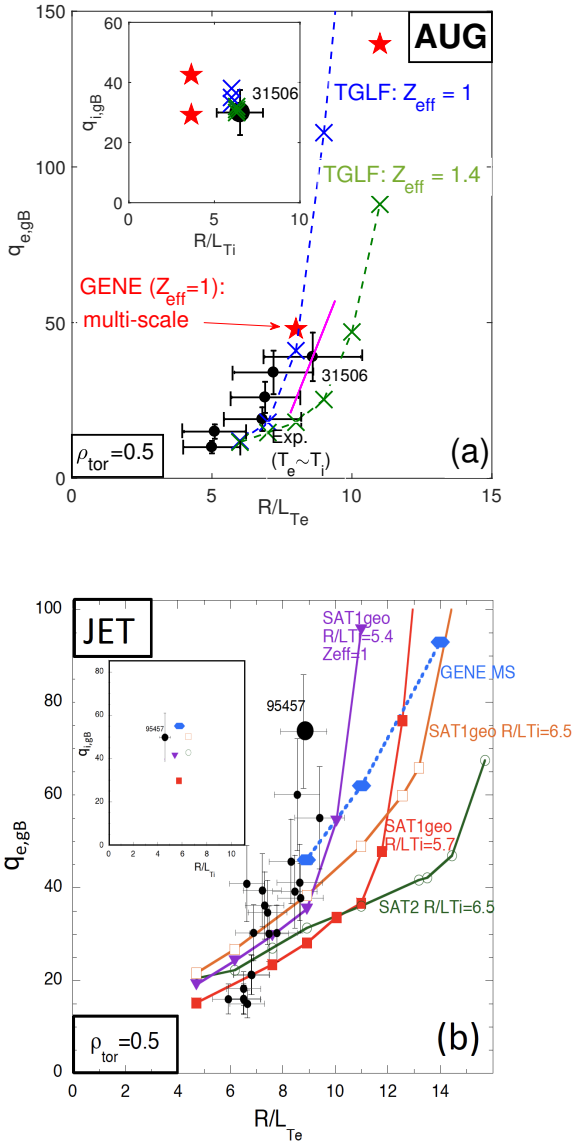

Figure 8. TGLF stand-alone fluxes, compared with exp. points and GENE multi-scale fluxes, for AUG (a) and JET (b). After [15] (b)

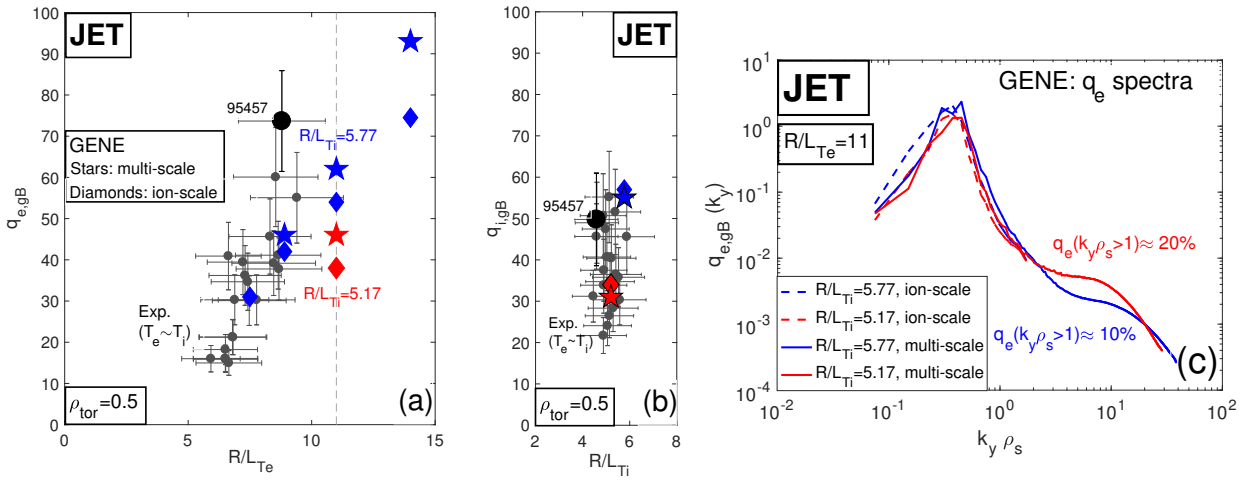

Figure 7. Multi-scale GENE electron heat flux in gB units $q_{e,gB}$ vs R/L_{Te} (stars), compared with the corresponding ion-scale fluxes (diamonds), for JET case, considering the two values $R/L_{Ti} = 5.17$ (red) and $R/L_{Ti} = 5.77$ (blue), which allow to match the experimental q_i at the two extremes of its error bar. Corresponding ion heat flux in gB units $q_{i,gB}$ vs R/L_{Ti} in (b). (c) Electron heat flux spectra in gB units $q_{e,gB}(k_y)$, corresponding to the simulations at $R/L_{Te} = 11$, comparing the runs with $R/L_{Ti} = 5.17, 5.77$ following the same color code of (a)/(b). After [15].

The situation is different for JET (Fig.8 (b)). The stiffness of SAT1-geo in the TEM part of the curve is a bit lower than in experiment and in GENE, but overall acceptable, whilst that of SAT2 is significantly underestimated. Both models feature an ETG wall at quite large values of R/L_{Te}, so that they miss reproducing the experimental uppermost points by a factor > 2 in $q_{e,gB}$, as for the GENE multi-scale, which however does not feature an ETG wall. As a matter of fact, the only case where the TGLF SAT1-geo curve approaches the experimental data also in the uppermost region is that with $Z_{\rm eff} = 1$, which however is experimentally unrealistic. One should note that for JET, since TGLF $q_{i,gB}$ is significantly underestimated at the nominal R/L_{Ti}, also cases with increased R/L_{Ti} (to match $q_{i,gB}$) are shown, which is key for a correct reproduction of multi-scale interactions.

It has to be pointed out that for both AUG and JET cases the impact of $Z_{\rm eff}$ on the up-shift of the 'ETG wall' is larger than what one would expect looking at the results of Fig.3, based on the simple γ/k_y criterion for ETG impact on fluxes.

Due to the strong sensitivity of the TGLF simulations to $Z_{\rm eff}$ for the JET case, and due to the lack of GK multi-scale simulations with impurities to compare with, a more detailed study of the effect of impurities for this case has been pursued in [15], performing TGLF scans of $q_{e,gB}$ vs R/L_{Te}, and considering the real impurity mix: Be, C, Ne, Ni and W, also separating light and heavy impurities. It results that TGLF gets closer to the experimental data, almost explaining them, only when the heavy impurities are neglected. This remains to be understood, with new multi-scale GK runs when resources will be available, where light and heavy impurities are treated separately, and not lumped together in a single C effective impurity as in the multi-scale GK runs presented in Sect.V.

VII. CONCLUSIONS

A collection and comparison of similar experiments that have been performed at the three tokamaks TCV, AUG and JET, assessing the impact of ETG modes on the electron heat transport, is presented in the paper. The experimental observations, coming from dedicated plasma pulses, are interpreted with the help of numerical simulations, including very computationally heavy nonlinear multi-scale gyrokinetic runs. The same experimental framework has been applied to the different machines, consisting in performing steady state electron heat flux scans ($q_{e,gB}$ vs R/L_{Te}), obtained varying the electron heating radial deposition. This is done to study the electron temperature stiffness and test the possible presence of an ETG wall, also varying the ion/electron heating power ratio since it impacts the ETG linear threshold. When available (TCV and AUG), these data are confronted with a perturbative analysis based on ECH radio-frequency modulation, which allows an independent determination of the stiffness. Only the JET case presents experimental points with sufficiently high $q_{e,gB}$ to be compatible with an ETG wall. They are obtained for a heat flux scan with $T_e \sim T_i$. TCV and AUG lack such high $q_{e,gB}$ data, but they feature ECH modulation, which indicates that the experimental points with $T_e \sim T_i$ and largest R/L_{Te} are compatible with high ETG stiffness. Therefore, in the three tokamaks the resulting experimental picture is that ETGs could impact q_e for cases with $T_e \sim T_i$ and sufficiently high R/L_{Te}, obtained by a conjunction of electron and ion heating, which is in line with the actual theoretical understanding of ETGs.

Experimental data are confronted with linear, nonlinear ion-scale and multi-scale gyrokinetic GENE simulations and stand-alone TGLF quasi-linear runs. Linear GENE simula-

tions indicate different regimes at ion scales for the reference cases of TCV and AUG/JET (TEM-dominant for TCV and ITG-dominant for AUG and JET), while ETGs dominate at electron scales for all cases. Linear simulations, based on a simple criterion applied to the eigenvalue spectra, allow to make a preliminary prediction of the impact of ETGs on q_e. The results confirm that the already mentioned experimental cases with $T_e \sim T_i$ and high R/L_{Te} are good candidates to show an ETGs role. In particular, the effect of the fast ions which are produced by the NBI, stabilizing the TEM-dominant ion scales, plays an important role for the TEM-dominant reference TCV case, while for the the ITG-dominant AUG and JET cases a larger role is predicted for ETGs when R/L_{Ti} is decreased (matching q_i with ion-scale nonlinear simulations within its error bar), consistently with an expected reduced ITG nonlinear zonal flow damping of ETGs. Finally, a stabilising effect is predicted for Z_{eff} for ETGs, consistently with the linear theory, which is larger at larger R/L_{Ti}.

Then, nonlinear ion-scale GK simulations have been performed. The results show that a lack of electron heat flux is observed in GK when compared with experiment for the TCV and JET cases. In particular, a synergy of fast ions and $E \times B$ shearing, both due to NBI, strongly stabilizes the ion scales for the TCV case. A lack of electron stiffness is observed for all the TCV, AUG and JET cases. In particular, for JET it is possible to match the flux level by varying the input parameters within error bars, but not the stiffness.

As a third step, nonlinear multi-scale GK simulations have been performed for the AUG and JET cases (for TCV possible global effects need to be modelled with a global multi-scale simulation with fast ions and $E \times B$ shearing, which is not computationally feasible). For AUG the multi-scale results allow to explain the experimental stiffness as coming from ETGs, although a caveat is that impurities have been neglected in the multi-scale simulations due to computational resources constraints. For JET the impurities have been taken into account, and the GK fluxes do not explain both the experimental flux levels and stiffness, with ETGs that are found to play a minor role for this case. Even a multi-scale simulation that has been performed for R/L_{Te} larger than the experimental one and lowering R/L_{Ti} down to the lowest possible value compatible with matching q_i with ion-scale runs, predicts a moderate role for ETGs, but q_e is even smaller than for the corresponding simulation with larger R/L_{Ti}, due to the reduced contribution of ITG-dominant ion scales. A possible alternative explanation of the JET case could come from cross-scale effects like those observed in [2], but they seem incompatible with the observed high ion stiffness.

Since due to a lack of computational resources it was not possible to investigate in detail the effect of the impurities on the results, repeating the heavy multi-scale runs adding them for AUG or removing them for JET, a quasi-linear analysis has been performed using the stand-alone version of TGLF. The results indicate that the effect of impurities is not negligible for AUG but it is possible to explain the experimental data with or without adding them, within experimental error bars. For JET it is possible to get close to explain the experimental data with TGLF only neglecting heavy impurities, that have a large impact on the position of the ETG wall in the $q_{e,gB}$ vs R/L_{Te} plane.

To further test the role of ETGs, sensitivity scans in the multi-dimensional parameter space should be performed with NL multi-scale GK simulations (presently not possible due to their computational cost). Moreover, density and possibly temperature fluctuations should be experimentally measured at electron scales, and compared with synthetic diagnostics applied to multi-scale GK runs. Finally, more conclusive results on the impact of impurities on ETGs are needed, in particular by performing more multi-scale GK simulations with impurity species, possibly separating the effects of light and heavy impurities. This could be useful in turn to better calibrate quasi-linear models like TGLF vs GK and improve the reliability of plasma profiles prediction in cases that are compatible with ETG relevance.

ACKNOWLEDGEMENTS

This work has been carried out within the framework of the EUROfusion Consortium and has received funding from the Euratom research and training programme 2014-2018 and 2019-2020 under grant agreement number 633053. The views and opinions expressed herein do not necessarily reflect those of the European Commission. O. Sauter was supported in part by the Swiss National Foundation. We acknowledge the CINECA award under the ISCRA initiative, for the availability of high performance computing resources and support. Part of the simulations presented in this work were performed at the COBRA HPC system at the Max Planck Computing and Data Facility (MPCDF), Germany. This work was also conducted under the auspices of the ITPA Topical Group on Transport & Confinement. Fig.1 (a), Fig.2 (a) and Fig.4 (a) are adapted, with permission, from [4].

REFERENCES

[1] Dorland W., Jenko F., Kotschenreuther M., and Rogers B.N., 2000 *Phys. Rev. Lett.* **85** 5579

[2] Howard N.T., Holland C., White A.E., Greenwald M. and Candy J., 2016 *Nucl. Fusion* **56** 014004

[3] Bonanomi N., Mantica P., Citrin J., Goerler T., Teaca B., and JET Contributors, 2018 *Nucl. Fusion* **58** 124003

[4] Mariani A., Mantica P., Brunner S., Fontana M., Karpushov A., Marini C., Porte L., Sauter O., the TCV Team and the EURO-

fusion MST1 Team, 2019 *Nucl. Fusion* **59** 126017
[5] Ryter F., Angioni C., Dunne M., Fischer R., Kurzan B., Lebschy A., McDermott R.M., Suttrop W., Tardini G., Viezzer E., 2019 *Nucl. Fusion* **59** 096052
[6] Maeyama S., Idomura Y., Watanabe T.-H., Nakata M., Yagi M., Miyato N., Ishizawa A., and Nunami M., Phys. Rev. Lett. 114 (2015) 255002
[7] Marinoni A., Pinsker R.I., Porkolab M., Rost J.C., Davis E.M., Burrell K.H., Candy J., Staebler G.M., Grierson B.A., McKee G.R., 2017 *Nucl. Fusion* **57** 126014
[8] Holland C., Howard N.T. and Grierson B.A., 2017 *Nucl. Fusion* **57** 066043
[9] Jenko F., Dorland W., and Hammett G.W., 2001 *Phys. Plasmas* **8** 4096
[10] Jenko F., Dorland W., Kotschenreuther M., and Rogers B.N., 2000 *Phys. Plasmas* **7** 1904
[11] Görler T., Lapillonne X., Brunner S., Dannert T., Jenko F., Merz F., and Told. D., 2011 *J. Comput. Phys.* **230** 7053
[12] Peeters A.G., Camenen Y., Casson F.J., Hornsby W.A., Snodin A.P., Strintzi D., Szepesi G., 2009 *Comput. Phys. Commun.* **180** 2650
[13] Staebler G.M., Candy J., Howard N.T., and Holland C., 2016 *Phys. Plasmas* **23** 062518
[14] Bonanomi N. *et al.*, to be submitted
[15] Mantica P. *et al.*, submitted to *Nucl. Fusion*
[16] Lütjens H., Bondeson A., Sauter O., 1996 *Comput. Phys. Commun.* **97** 219
[17] Brix M., Hawkes N.C., Boboc A., Drozdov V., Sharapov S.E., and JET-EFDA Contributors, 2008 *Rev. Sci. Instrum.* **79** 10F325
[18] Staebler G.M., Howard N.T., Candy J., and Holland C., 2017 *Nucl. Fusion* **57** 066046
[19] Staebler G.M., Candy J., Belli E.A., Kinsey J.E., Bonanomi N., and Patel B., 2021 *Plasma Phys. Control. Fusion* **63** 015013